



## Modular construction mechanics of a European pressurized reactor steel containment liner\*

Jia-chuan YAN<sup>†1,2</sup>, Xiao-fei JIN<sup>3</sup>, Feng QIN<sup>4</sup>, Zheng LI<sup>5</sup>, Feng FAN<sup>1,2</sup>, Jin-ping OU<sup>1,2</sup>

<sup>(1)</sup>Key Lab of Structures Dynamic Behavior and Control of the Ministry of Education, Harbin Institute of Technology, Harbin 150090, China)

<sup>(2)</sup>School of Civil Engineering, Harbin Institute of Technology, Harbin 150090, China)

<sup>(3)</sup>China Construction First Engineering Division Corporation Limited, Beijing 101300, China)

<sup>(4)</sup>Country Garden, Foshan 528312, China)

<sup>(5)</sup>China Construction Second Engineering Bureau Nuclear Power Plants Branch, Shenzhen 518034, China)

<sup>†</sup>E-mail: jiachuanyan@163.com

Received Feb. 10, 2016; Revision accepted Oct. 4, 2016; Crosschecked May 15, 2017

**Abstract:** A European pressurized reactor (EPR) steel containment liner structure is comprised of the cylinder part and the dome part. An introduction of the steel liner structure is presented, followed by studies on the key mechanical features of the construction process using a refined finite element method. The steel liner was divided into several modules and then assembled during construction. Firstly, the equipment structure used to hoist the liner module was optimized, the lifting lug was analyzed using a multi-scale finite element model; the wind speed limit during lifting was also studied. Subsequently, the effect of internal forces during assembly between the liner modules, the lateral pressure of fresh concrete, the non-uniform temperature load, and the wind load on the cylinder module was analyzed. According to the time-varying structural performance during continuous concrete pouring and the hardening construction, an “overlapping element and birth-death element” technique was adopted to analyze the deformation and stress of the long-span steel dome liner. In addition, the stability-bearing capacities of the dome structure during construction were also studied, which took into consideration the effect of the initial geometrical imperfections and the elasto-plasticity of the material. This study presents a reference in terms of the mechanics of the construction scheme and the safety of such a type of structure.

**Key words:** Containment; Construction mechanics; Steel liner; Overlapping element; Birth-death element  
<http://dx.doi.org/10.1631/jzus.A1600136>

**CLC number:** TU393.3

### 1 Introduction

The Taishan nuclear power project in Guangdong province of China is a third generation advanced nuclear power technology project jointly developed and constructed by Chinese and French

companies. It has the world's largest capacity for nuclear power generating units (People's Daily, 2009). Following Finland and France, it is the third European pressurized reactor (EPR) nuclear power plant under construction (WNN, 2013a; de Clercq, 2014). The EPR nuclear power plants are not yet in service. The standard for the construction technology of the Taishan EPR nuclear power plant is based mainly on European and French EPR technology models (WNA, 2010; WNN, 2013b). Many construction technologies from the EPR nuclear power plants are being used in China for the first time (IAEA, 2012a; 2012b). In order to form an independent EPR nuclear power plant construction

\* Project supported by the China State Construction Engineering Corporation Funded Project (No. CSCEC-2008-Z-17), the National Natural Science Foundation of China (No. 51308155), the Fundamental Research Funds for the Central Universities of China (No. HIT.NSRIF.2014100), and the China Postdoctoral Science Foundation Funded Project (Nos. 2013M541389 and 2015T80355)

 ORCID: Jia-chuan YAN, <http://orcid.org/0000-0002-2781-9046>

© Zhejiang University and Springer-Verlag Berlin Heidelberg 2017

technology in China, it is necessary to understand, assimilate, and be able to recreate the imported construction technology.

As an important component for resisting external loads and providing airtight integrity, the containment building is the final barrier against radioactive release and it is essential for the safety of the nuclear power plant (Fib Task Group on Containment Structures, 2001). The EPR containment building is a double-layer shell structure, i.e., inner and outer containment structures, as shown in Fig. 1 (ASN, 2015). The inner containment structure is composed of a pre-stressed concrete cylinder and a pre-stressed concrete dome, which is entirely lined on the inside surface with a steel panel to ensure the seal for the pressure boundary. The outer containment structure is a reinforced concrete structure, which is designed to resist external hazards, such as an aircraft impact (von Riesemann and Parks, 1995; Becue *et al.*, 2005).

Research on the mechanical properties of containment structures under extreme loads, such as a thermal load caused by a loss of coolant accident (LOCA), seismic load, internal pressure, and impact load, has attracted a considerable amount of interest

(Zhang, 2009; Marques, 2010). Extensive experimental studies have been conducted to investigate the mechanical properties of the containment structure under internal pressurization. Rizkalla *et al.* (1984) tested a 1:14 scale pre-stressed concrete structure model of a Canadian reactor containment structure. The model has high ductility under the action of internal pressure. Twidale and Crowder (1991) carried out a pressure test on a 1:10 scale pre-stressed concrete model of the Sizewell B containment structure. At Sandia National Laboratories (SNL), a 1:6 scale reinforced concrete containment model was pressurized to failure (Horschel, 1988; 1992). Hessheimer *et al.* (2003) conducted a pressure test on a 1:4 scale model of the pre-stressed concrete containment structure of Unit 3 at the Ohi Nuclear Power Station. Parmar *et al.* (2014) tested a 1:4 scale model of the pre-stressed concrete inner containment structure of Tarapur Atomic Power Station Units 3 and 4. These experimental results have been used as references for the validation of the numerical analyses around the world.

With the advancement of computing technology, it is now possible to conduct comprehensive numerical analyses on the mechanical properties of

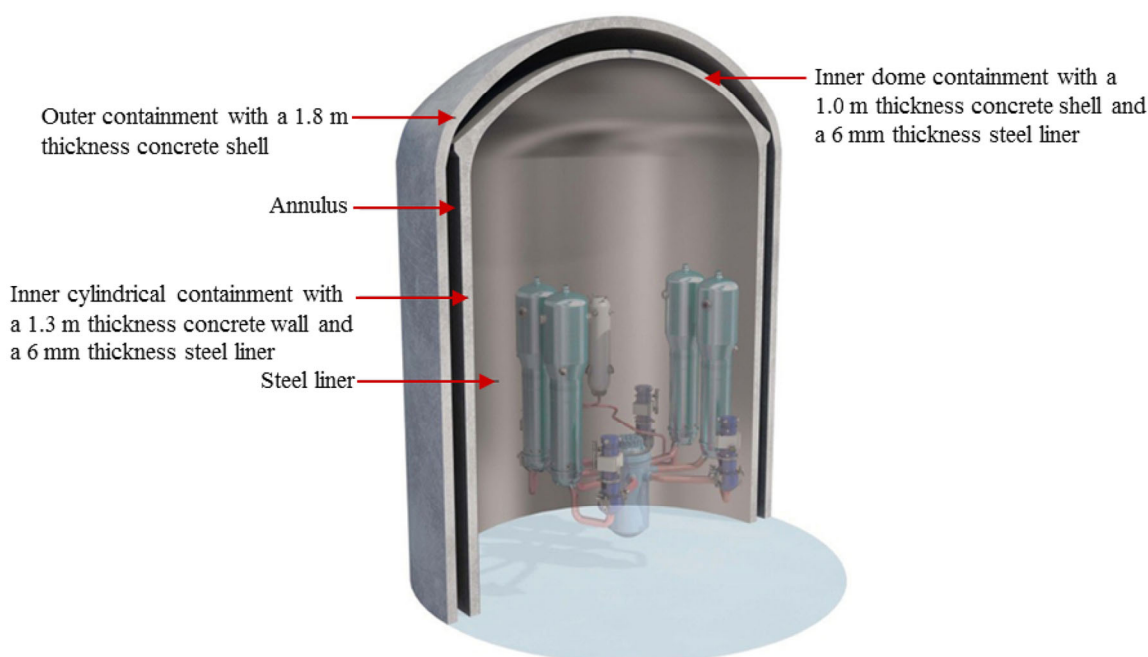


Fig. 1 Containment structure for an EPR reactor building (ASN, 2015)

containment structures. A series of numerical simulations were conducted to simulate the pressure test of the 1:4 scale pre-stressed concrete containment vessel (PCCV) model at Sandia National Laboratories, USA and to predict the ultimate load capacity for the design of the PCCV (Yonezawa *et al.*, 2002; Basha *et al.*, 2003; Lee *et al.*, 2004; Kwak and Kwon, 2016; Shokoohfar and Rahai, 2016). The influence of the pre-stress loss on the mechanical properties of the containment structures was also investigated. Anderson (2005) showed measurements for pre-stress loss in tendon force for 30 years and proposed models to predict pre-stress loss. Lundqvist and Nilsson (2011) showed the pre-stress loss obtained from two Swedish containments during in-service inspections, and modified the prediction models for the shrinkage of concrete. Hu and Lin (2016) carried out a finite element analysis to predict ultimate pressure capacity and the failure mode of a PCCV under long-term pre-stressing loss. Kim *et al.* (2013) developed a probabilistic model for the long-term degradation of tendon force, and performed a reliability evaluation for nuclear containment.

For the construction of a nuclear power plant, modular construction technology has been widely adopted, which means that modules of certain types of equipment, pipelines, electrical instruments, and the steel structure, are prefabricated in the workshop and then assembled on site to form the whole structure. During the assembly procedure, large lifting equipment is used. Because these large modules can be separated from each other and fabricated in many different regions or areas, the engineering construction, installation, device debugging, and other operations can be carried out simultaneously and independently in those isolated regions. Modular construction technology turns the old style of a dispersed labor-intensive construction mode into an intensive and organized factory construction mode, and optimizes the logic of constructing different specialized parts at the same time, which makes the construction of the nuclear power plant more systematic and efficient (Lapp and Golay, 1997).

Modular construction technology results in “giant structure modules”, which is a method that was applied to the steel liner for the containment building at the Taishan nuclear power plant. The steel liner is comprised of several modules of different heights,

including a number of cylinder modules (weighing up to 85 t) and a dome module (weighing around 240 t). These modules were assembled segment by segment on site. Each module was lifted into position, and welding was used to connect the upper module and the lower module. By taking advantage of this “building blocks” construction style, the work in the civil engineering domains and the work in equipment installation could be carried out simultaneously. The steel cylinder liner is used naturally as the lateral formwork for concrete pouring on the containment cylinder wall, and the steel dome liner is also used as a bottom formwork for concrete pouring on the containment dome.

Despite the extensive experimental and numerical studies performed on scaled containment structures, the mechanics of the containment structure during the actual process of modular construction has not yet been investigated systematically. In this paper, three key problems were proposed and analyzed to investigate the mechanical properties of the steel liner during the modular construction process of the containment structure.

## 2 Key problems

The inner containment cylinder has an inner diameter of 46.8 m and a height of 48.267 m. The thickness of the inner containment cylinder wall is 1.3 m. There are three counterfort columns around the cylinder containment. The portion above +43.917 m is the dome of the inner containment structure. For the dome, the inner radius, the elevation of the highest point, and the thickness are 32 m, +58.509 m, and 1.0 m, respectively. The inner radius of the ring beam, which connects the dome and the cylinder, is 8 m. The strength grade of the concrete is C60/75. C60 represents the concrete compressive strength per the European standard, which adopts a cylinder specimen with a size of 160 mm×320 mm; C75 represents the concrete compressive strength per the Chinese standard, which adopts cube specimens with a size of 150 mm×150 mm×150 mm. The steel liner uses steel plate with a grade of P265GH and a thickness of 6.00 mm. The cross section of the steel angle stiffener set on the steel dome liner is L200×100×10 (mm) (latitudinal and longitudinal) and L70×50×6

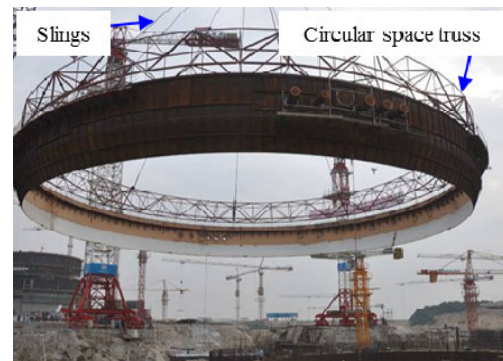
(mm) (longitudinal). The cross section of the steel angle stiffener set on the steel cylinder liner is 2L120×80×10 (mm) (circular) and L70×50×6 (mm) (vertical).

The steel liner is thin but with a large span, which means the stability safety during modular construction is of great importance. Therefore, several issues require careful consideration to guarantee the stability safety.

Firstly, a circular space truss is the equipment used to lift the steel cylinder liner modules. The circular space truss should be as light as possible to reduce the crane load and should be stiff enough to limit deformation during the lifting process, as shown in Fig. 2a. The dome module of the steel liner is lifted directly by slings, as shown in Fig. 2b. When the overall deformation requirement is satisfied during the lifting process, the maximum stress concentration at the lifting lug should prevent the occurring of the local plastic deformation. The dome will sway due to wind load during the lifting process, which results in additional wind load on the crane. Therefore, the safe wind speed allowed during the lifting process should be verified.

Secondly, the steel cylinder liner modules are assembled by welding multiple prefabricated standardized steel panels on site. A cylinder module is lifted as a whole into position and welded to the lower cylinder module. The average height of the cylinder modules is 5.75 m. The average height of the concrete poured at any given time is 2.5 m. Given that the steel cylinder liner has a height of 46.8 m and a thickness of 6.00 mm, concrete pouring would result in considerable lateral pressure on the steel liner, and the resulting deflection of the steel liner should satisfy the tolerance requirements. Meanwhile, the stress and deformation of the steel cylinder liner will be influenced by internal forces during assembly between the cylinder modules, wind load, temperature difference between the sunny side and the shady side, or other factors. Therefore, the height of the steel cylinder liner module and the height of the concrete pouring at any time should be optimized, to ensure safe and accurate modular construction.

Thirdly, the steel dome liner module is assembled on the ground, and then is lifted and installed. When the concrete is poured on the dome, the steel dome liner module acts as the bottom formwork for the concrete. However, due to construction difficulty,



(a)



(b)

**Fig. 2 Lifting the steel liner modules**

(a) Lifting of the cylinder module (Enformable Nuclear News, 2011); (b) Lifting of the dome module (Nuclear Engineering International, 2009)

no support or brace can be installed to support the steel dome liner module. The concrete on the dome is poured via different layers and at different times, which means that each layer of concrete is poured when the previous concrete layer has obtained certain strength. As the concrete strength grows gradually, the concrete layers contribute to the resistance and stability of the whole dome gradually. In this way, supports or braces for the steel dome liner module are eliminated by taking full advantage of the strength of the concrete.

For the thin shell of the large span, the stability is the controlling factor for structural safety. According to the Chinese code “Specification for Design of Reinforced Concrete Shell Structures” (JGJ 22-2012) (MOHURD, 2012b), an analysis of the structure at different construction stages is of vital importance, since accidents often occur during the construction phase when the whole structure has not yet been formed.

### 3 Lifting of steel liner modules

#### 3.1 Mechanical optimization analysis of the circular space truss lifting equipment

The steel cylinder liner modules are hoisted using the circular space truss lifting equipment. Since multi-point flexible connections are used between the circular space truss and the modules, the stiffness of the circular space truss must be much greater than that of the steel liner modules. Given that the lifted module will be welded to the lower module which is already set up in place, the vertical deformation and radial deformation of the circular space truss must be less than 50 mm, which is the requirement in the Chinese code “Code for Design of Steel Structures” (GB50017-2003) (MOHURD, 2003).

In the Taishan nuclear power plant project, a space truss with a quadrilateral cross section is used as the circular space truss, and the dimensions of the cross section are 2.60 m×2.60 m. The outer diameter of the circular space truss is 23.4 m, and the inner diameter of the circular space truss is 20.8 m. Five different cross sections of steel pipes are used, including  $\Phi 160 \times 12$ ,  $\Phi 150 \times 8$ ,  $\Phi 120 \times 6$ ,  $\Phi 90 \times 6$ , and  $\Phi 60 \times 4$  (mm). The diameter of the cross section of the slings is 40 mm, and the tensile strength of the material for the sling is 1670 MPa. Eight hoisting points, which are uniformly distributed on the upper chord of the inner ring, are set on the circular space truss. In the circular space truss, the uniformly distributed joints between the lower chord of the outer ring and the vertical members are taken as the lifting points to connect with the steel cylinder liner modules. The length of each sling is 40.0 m, and the height of the lifting hook above the plane of the upper chord is 34.0 m.

The ANSYS software is used for modeling and analysis (ANSYS Inc., 2012). The truss member is simulated with the LINK180 element. The slings are simulated by the LINK180 element, and the LINK180 elements simulating the slings are set in tension only. The steel liner is simulated with the SHELL181 element, as shown in Fig. 3.

The weight of the biggest steel cylinder liner module is 85.0 t; the lifting dynamic factor for structural analysis is 1.40. For most of the truss members, the simulated stresses are less than 100 MPa, which means the stress level as a whole is low. The maxi-

imum simulated stress of the truss members is 239 MPa, which is near the hoisting points. The circular shrinkage deformation of the truss is 11.0 mm. If the vertical rigid body displacement caused by the deformation of the slings is removed, as shown in Fig. 4, the maximum vertical displacement of the truss is 16.0 mm, at the middle of the two adjacent hoisting points on the upper chord, which satisfies the requirement for the deformation-span ratio, i.e.,  $11.0 \text{ mm}/18.0 \text{ m} < 1/250$  (the span between the upper hoisting points is about 18.0 m).

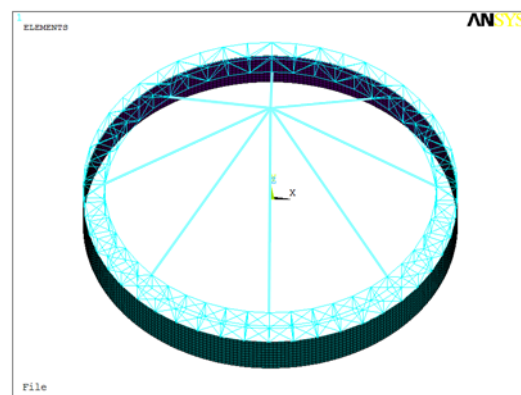


Fig. 3 Circular space truss model with the quadrilateral cross section that hoists a cylinder module

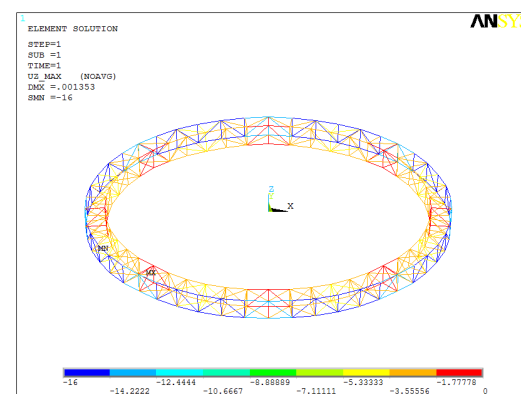
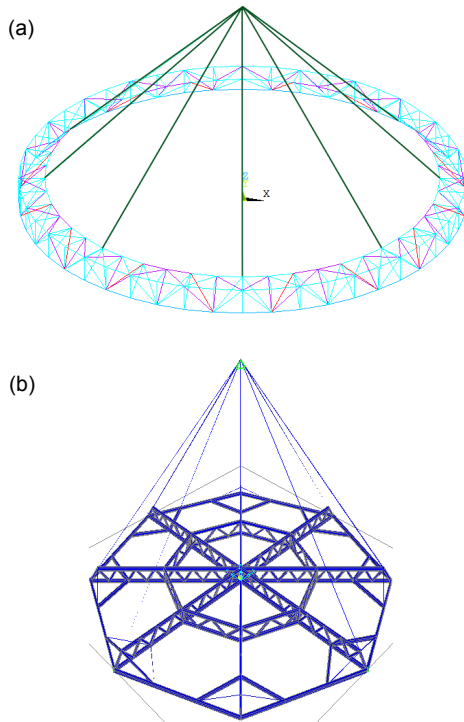


Fig. 4 Vertical displacement of the circular space truss without rigid displacement (unit: mm)

Based on analysis of these parameters, two types of new structures are proposed for the lifting equipment. The first one is a circular space truss with a triangular cross section, and the other one is a composite structure of plane trusses, as shown in Fig. 5. The results show that these two new types of

structures can satisfy the stress and deformation requirements during the lifting process. Compared with the lifting equipment used in practical engineering (a circular space truss with quadrilateral cross section), a circular space truss with a triangular cross section exhibits better mechanical properties, and the consumption of steel can be reduced by 20%.



**Fig. 5 Two types of circular space truss**

- (a) Circular space truss with a triangular cross section;  
 (b) Composite structure of plane trusses

### 3.2 Mechanical analysis of lifting of the dome module

The type of material for the steel dome liner module is P265GH. The elastic modulus, average yield strength, Poisson's ratio, and density of the steel liner are  $2.1 \times 10^5$  MPa, 320 MPa, 0.28, and  $7850 \text{ kg/m}^3$ , respectively (CEN, 2003; 2005). The steel plate is simulated by the SHELL181 element, and the angle steel stiffeners are simulated by the BEAM188 element. The inclined angle between the slings and the horizontal plane is  $50^\circ$ , as shown in Fig. 6.

The weight of the steel dome liner module is 260 t. The lifting dynamic factor is 1.15. Fig. 7

shows the displacement of the dome module when it is lifted. The maximum displacement in the horizontal direction is 0.80 mm. The maximum vertical deformation is only 1.30 mm, without the vertical rigid body displacement caused by the elongation of the sling.

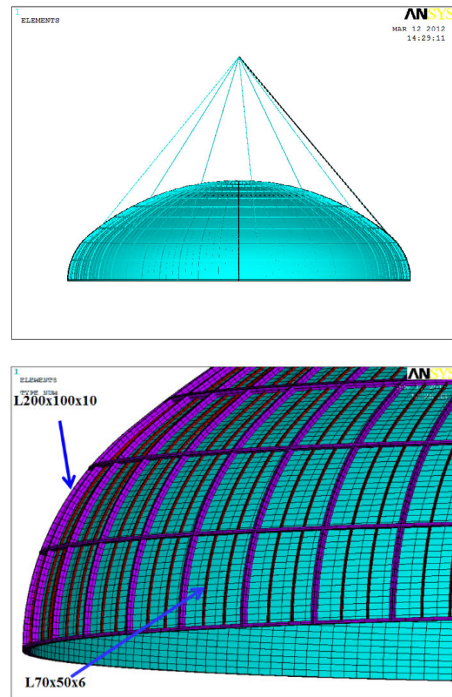


**Fig. 6 Analysis model for lifting the dome module**

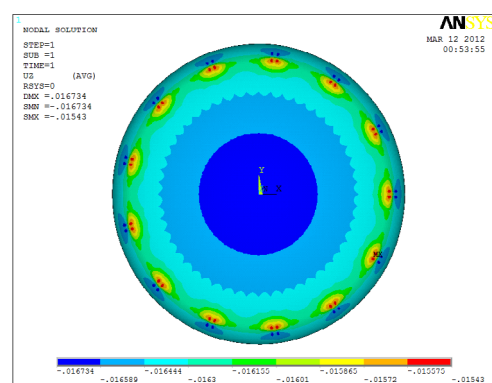


**Fig. 7 Vertical displacement of the steel dome liner with rigid body displacement (unit: m)**

In order to obtain structural stresses of the zone near the hoisting points, the ABAQUS software was used to conduct a multi-scale finite element analysis

(ABAQUS Inc., 2012). Based on the symmetry of the structure, a partial structure was modeled. The steel plate is simulated by the S8R5 shell element, and the stiffeners are simulated by the B31 beam element. Only the stiffeners near the lug and the lug itself are simulated by the shell element. A symmetric boundary is applied, and along the direction of the sling, the fixed boundary is applied on the lifting lug. The gravity load is taken as the calculation load, and the dynamic factor is 1.15. The results show that the maximum displacement is only 1.22 mm, and the maximum von Mises stress of the lifting lug is 115 MPa, which is much less than the average yield stress, as shown in Fig. 8.

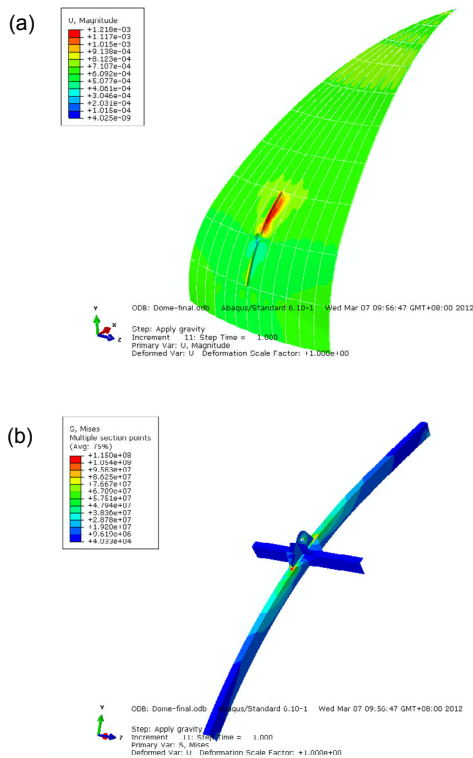


**Fig. 8 Joint analysis of the steel dome liner module**  
 (a) Deformation (unit: m); (b) von Mises stress of the lifting lug (unit: Pa)

### 3.3 Working wind load analysis

The area on the windward side of the dome module  $A$  is large (about  $499.8 \text{ m}^2$ ). The large wind load would result in deflection, and consequently lead to additional wind load, which can increase the lifting load. Furthermore, excessive deflection is

easy to induce in a collision between the dome and the crane arm.

Taking the weight of the steel wire ropes and other lifting appliance into consideration, the lifting weight is about  $240 \text{ t} \times 1.10 = 264 \text{ t}$ . The rated lifting weight of the crane is  $300 \text{ t}$  (load rate is  $88.0\%$ ). In order to ensure safety during lifting, the additional wind load during lifting should be controlled to less than  $1.00\%$  of the rated lifting weight, i.e.,  $F = 300 \text{ t} \times 1.00\% = 3.0 \text{ t}$ . Subsequently, the deflection angle between the lifting hook and the vertical line is  $\theta = \arctan(3/264) = 0.65^\circ$ . The deflection is very small and satisfies the requirement. The wind load is calculated as

$$F = \mu_s \mu_z w_0 A, \tag{1}$$

where  $A = 500 \text{ m}^2$ , the wind load shape coefficient  $\mu_s$  is 1.2, the wind pressure height coefficient  $\mu_z$  is 2.10 (according to class A, 70.0–80.0 m high), the basic wind pressure  $w_0 = v_0^2 / 1600 \text{ (kN/m}^2\text{)}$ , and the wind speed  $v_0 \approx 6.17 \text{ m/s}$ .

Based on these calculations, the working wind speed should be controlled to within  $6.17 \text{ m/s}$  during the lifting of the dome module.

## 4 Construction mechanical performance of the steel cylinder liner modules

### 4.1 Finite element model

The concrete is simulated by the SOLID65 element in the ANSYS software; the reinforcement ratios per unit volume of corresponding latitude direction, longitude direction, and thickness direction for the different regions are set. The steel liner is simulated by the SHELL181 element, and the stiffeners of the steel liner are simulated by the BEAM188 element, as shown in Fig. 9. The beam elements and shell elements share the nodes. The cross section of the beam element is offset in the finite element model, i.e., the limb tip of the steel angle is rigidly connected with the steel liner. Concrete elements and steel liner shell elements also share the nodes. Because the steel liner affixes to the solid concrete, and the meshing is relatively fine, the discordance effect of rotational degrees of freedom between the solid element and the shell element is ignored.

For an analysis of the whole construction process, the development of the elastic modulus of the concrete taking into account increasing age is considered. If the age of the concrete is more than 28 d, the elastic modulus equals that of the age of 28 d. The concrete elastic modulus at different ages is calculated using the method offered in Appendix B of the Chinese code “Code for Construction of Mass Concrete” (GB 50496-2009) (MOHURD, 2009).

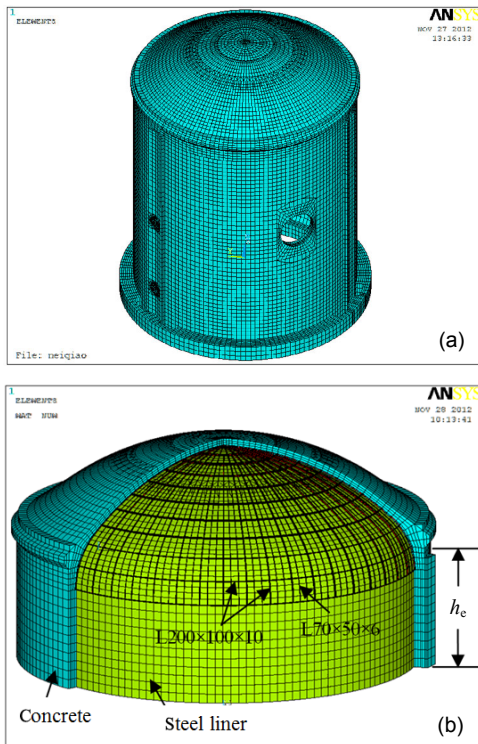


**Fig. 9** Finite element model of the inner containment structure

(a) Whole model; (b) Enlarged partial model.  $h_c$  is the relative elevation of the section to the bottom of the dome

## 4.2 Construction load analysis

1. The value for the lateral pressure of the concrete pouring on the steel cylinder liner is determined according to the Chinese code “Technical Code for Safety of Forms in Construction” (JGJ 162-2008) (MOHURD, 2008).

2. The value of the wind load is determined according to the Chinese code “Load Code for the Design of Building Structures” (GB 50009-2012) (MOHURD, 2012a), and the basic wind pressure is determined by the 10-year frequency.

3. The sun temperature difference between the sunny side and shady side of the steel cylinder liner during construction is determined according to the Chinese code “Load Code for the Design of Building Structures” (GB 50009-2012) (MOHURD, 2012a). Two temperature differences (5 °C and 10 °C) were considered.

4. The internal forces during assembly between the steel cylinder liner modules are calculated as follows.

The steel cylinder liner module is assembled with multiple steel plates through vertical welds. Before the final vertical seam is welded and closed, the circumference of the opening edge of the lower already-fixed steel cylinder liner should be measured (generally this process must be conducted at the same time every morning). Based on the measured circumference, the circumference of each subsequent steel cylinder liner module to be welded onto the lower already-fixed steel cylinder liner is adjusted, and the possible redundant length is cut off before the final seam is welded, to minimize the internal forces during assembly between the modules.

Because of the complexity of the actual operation, the preliminary assembly internal force cannot be completely eliminated, and is difficult to measure. The internal force during assembly can be considered as a kind of load. Then it is assumed that the load complies with extreme value type I distribution, and the probability distribution functions are as follows:

$$F(x) = \exp[-\exp(-a(x-k))], \quad -\infty < x < \infty, \quad (2)$$

$$a = \frac{1.2825}{\sigma_X}, \quad (3)$$

$$k = \mu_X - \frac{0.5772}{a}, \quad (4)$$

where  $F(x)$  is the preliminary assembly internal force,  $\mu_X$  and  $\sigma_X$  are the mean value and the mean squared error of the random variable  $X$ , respectively, and  $a$  and  $k$  are parameters which can be determined by Eqs. (3) and (4), respectively.

According to “ASME Nuclear Power Codes and Standards” (BPVC-III-2) (ASME, 2015), after the welding of a steel cylinder liner module, the maximum deviation between the cylinder modules should not exceed  $t/4$ , where  $t$  is the nominal thickness of

the thinner section at the connection part between modules. The butt weld between the cylinder modules is generally located 1.00 m above the concrete below where the deviation of the cylinder is assumed to comply with the extreme value type I distribution. The probability that the deviation of the cylinder exceeds  $t/4$  ( $6.0/4 \text{ mm}=1.5 \text{ mm}$ ) is less than 0.10%, and  $\mu_X=0$ . The values of  $a$  and  $k$  are taken as 6.9065 and  $-0.0836$ , respectively. In the finite element model, based on this probability distribution, the data are extracted randomly as a forced displacement applied on each node of the assembly location between the cylinder modules, in order to calculate the reaction force, i.e., the preliminary assembly internal force.

### 4.3 Construction load analysis

According to “ASME Nuclear Power Codes and Standards” (BPVC-III-2) (ASME, 2015), for the specified increment of height, the difference between the maximum and minimum cylinder diameters should not exceed 0.50%; the total perpendicular deviation of the steel liner between the springing line (the bottom line of the dome containment) and the bottom line of the cylinder containment structure should be less than 1/200 of the total height of the steel cylinder liner.

Four kinds of load conditions were analyzed, as shown in Table 1. In order to satisfy the accuracy introduced above and to keep the stress state of the structure in an elastic state, the correlation curve of the steel liner modular height and the maximum height of a concrete pouring at any time is shown in Fig. 10. The figure shows that, in order to reduce the hoisting workload of the steel liner modules and the subsequent construction period, the height of the steel cylinder liner module can be increased if the capacity of the crane is sufficient. For example, when the height of the steel cylinder liner module is 8.00 m, the height of the concrete pouring at that time can be increased to 4.10 m.

When the steel cylinder liner module is fabricated on site, its controlling perimeter is determined according to the top opening perimeter of the lower module already installed. Therefore, during the whole modular construction process, the assembly deviation of the steel cylinder liner modules will accumulate one by one. According to load condition 1 in Table 1, the “birth-death element” technique is used to simulate the whole construction process. The accumulated deviation at the springing line of the steel cylinder liner (the bottom line of the steel dome liner) is about 92.0 mm (i.e., the maximum radial displacement), which can meet the requirements for perpendicular accuracy.

## 5 Time-varying structural performance of the inner dome containment structure during construction

The construction sequence for pouring the concrete of the dome is shown in Fig. 11. The first layer of 20.0 cm thick concrete is poured on the steel dome liner (i.e., layer E in Fig. 11, the surrounding space by the steel angle L200×100×10 (mm) on the

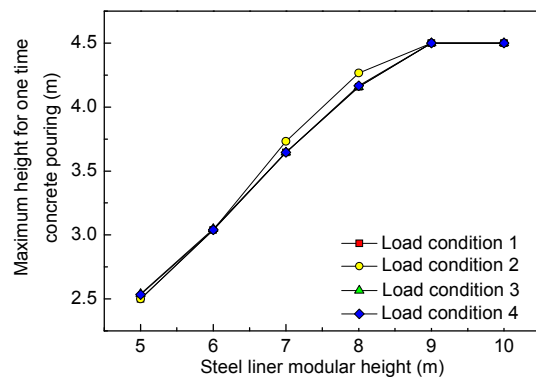
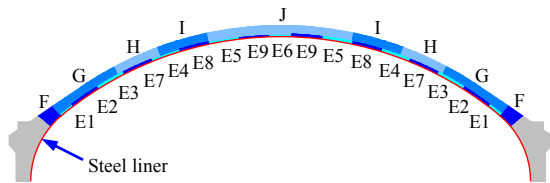


Fig. 10 Correlation curves for the steel liner modular height and the maximum height of a concrete pouring at any time

Table 1 Four kinds of load conditions

Load condition	Lateral pressure of the concrete pour	Preliminary assembly internal force	Wind pressure height (m)	Sunshine temperature difference (°C)
1	Considered	Considered	40	10
2	Considered	Considered	20	10
3	Considered	Considered	40	5
4	Considered	Considered	20	5

exterior of the steel dome liner). Subsequently, the second layer of 80.0 cm thick concrete is poured onto the first layer (i.e., layers G, H, I, and J in Fig. 11), in the order of E1→E2→F→E3→E4→E5→E6→E7→E8→E9→G→H→I→J. In accordance with the construction plan, the construction periods for layers E1 and E2 are both 15 d; the construction period for layer F is 97 d; the construction periods for layers E3, E4, E5, E6, E7, E8, and E9 are all 1 d. Then the construction period for laying pre-stressed reinforcement is 36 d. After that, layers G, H, I, and J are poured continuously, and the construction periods are 7 d, 14 d, 14 d, and 7 d, respectively.



**Fig. 11 Concrete pouring scheme for the inner dome containment structure**

The inner cylinder containment piece is associated to a cylindrical tube. Based on the linear-elastic theory of axisymmetric deformation of a long cylindrical tube, as the relative elevation of a cross section to the bottom cross section of the dome (+43.917 level) increases, shear force and the bending moment of this cross section will have a reduced effect on the bottom cross section of the dome (Timoshenko and Woinowsky-Krieger, 1959). When the relative elevation of the section to the bottom of the dome  $h_e$  meets Eq. (5), the shear force and the bending moment of the bottom cross section of the dome is only 4% of the shear force and the bending moment of this section. As the relative elevation of a cross section to the bottom cross section of the dome increases, the effect on the farther sections is negligible.

$$h_e = \pi \cdot \sqrt[4]{\frac{1}{3(1-\nu^2)}} \cdot \sqrt{R \cdot t}, \quad (5)$$

where  $R$  is the average radius of cylinder ( $R=24.1$  m);  $t$  is the thickness ( $t=1.30$  m);  $\nu$  is Poisson's

ratio ( $\nu=0.2$ ) (CEN, 2004). Therefore,  $h_e=14.1$  m. The inner containment structure is modeled from +32.0 m to the apex of the dome, and the translational and rotational degrees of freedom of the cross section at elevation +32.0 m are all constrained.

### 5.1 Structural stress and deformation analysis during construction

Construction mechanics belongs to the category of slowly time-varying mechanics (Wang, 2000). The geometry, the material properties, the supporting boundary, etc., of a structure during construction will change slowly over time. Thus, the structural construction process can be divided into a series of construction stages, and the structure at each construction stage is considered as a time-invariant structure. Therefore, the entire structural construction process is simulated by continuous solutions for these time-invariant structures.

In the past, the time-varying structural performance of a structure during the pouring of concrete was not explored systematically. Newly poured concrete in a construction project cannot participate in the resistance of the structure, and it is actually a kind of load for the structure. With the hardening of the concrete, the poured concrete becomes a part of the structure, and then it contributes to the resistance of the structure. As the concrete ages, the strength and elastic modulus of concrete in different parts of the structure will be different. The calculation for a load step must be based on the calculation for the previous step, and the "overlapping element and birth-death element" technique can be adopted to simulate the construction process of pouring concrete on the dome.

In the finite element model, a specified element is deactivated or "killed" when the birth and death capability is used. A deactivated element continues to exist in the model but contributes a near-zero stiffness (or conductivity, etc.) value to the overall matrix. Any solution-dependent state variables (such as stress, plastic strain, and creep strain) are set to zero. Deactivated elements contribute nothing to the overall mass (or capacitance, etc.) matrix. When the deactivated elements are reactivated, their stiffness, mass, loads, and so on, are set to original values within a zero strain (or thermal heat storage, etc.) state.

When newly poured concrete acts as the load, it is “killed” and the equivalent pressure load is applied on the steel dome. As the concrete ages, the concrete will harden, and the “overlapping element” technique is used for the simulation, which means that two independent overlapping elements are generated using the same nodes. Overlapping elements are “killed” and “reactivated” alternatively. When the concrete element is reactivated, its material properties are modified simultaneously according to the age of the current construction stage. At any stage, only one group of overlapping elements is reactivated. “Dead” elements drift correspondingly with the deformation of overlapping “live” elements under the action of load. When these elements are reactivated, they are recovered with new material properties on the cumulative structural deformation state, and no strain is recorded. The stress and strain state of other structural elements still remains in the state of previous load step. Then a mechanical analysis of the overall structure is conducted at the current load step. In this way, the calculation for a load step is based on the calculation for the previous step, for the whole process of pouring and hardening of the concrete.

During the construction process, the deformation check of the steel dome liner comprises the global geometry inspection and the local geometry inspection. The global geometry inspection is performed before and after pouring the concrete for the first 20 cm thickness of concrete. It consists of checking whether the dome liner is located between two surfaces,  $\pm 50$  mm from the theoretical surface. The local geometry inspection  $f$  should meet the following requirements (Fig. 12):

$$f \text{ (mm)} < 20 \times L^2 \text{ (m)}, \tag{6}$$

$$f = \frac{f_1 + f_2}{2} < 20 \text{ mm}, \tag{7}$$

where  $L$  is the minimum distance between the ribbed stiffeners of the steel dome liner, and  $f_1$  and  $f_2$  are the local geometric imperfections measured from the adjacent ribbed stiffeners, respectively, as shown in Fig. 12.

The vertical displacement and von Mises stress of the steel liner at each construction stage are

shown in Figs. 13–25. The position of maximum vertical displacement and the von Mises stress of the

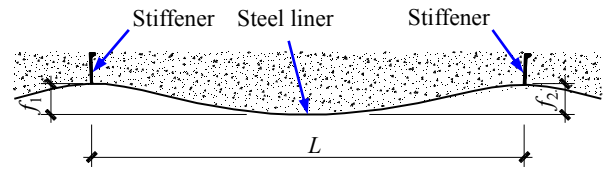


Fig. 12 Local geometry inspection of the steel liner

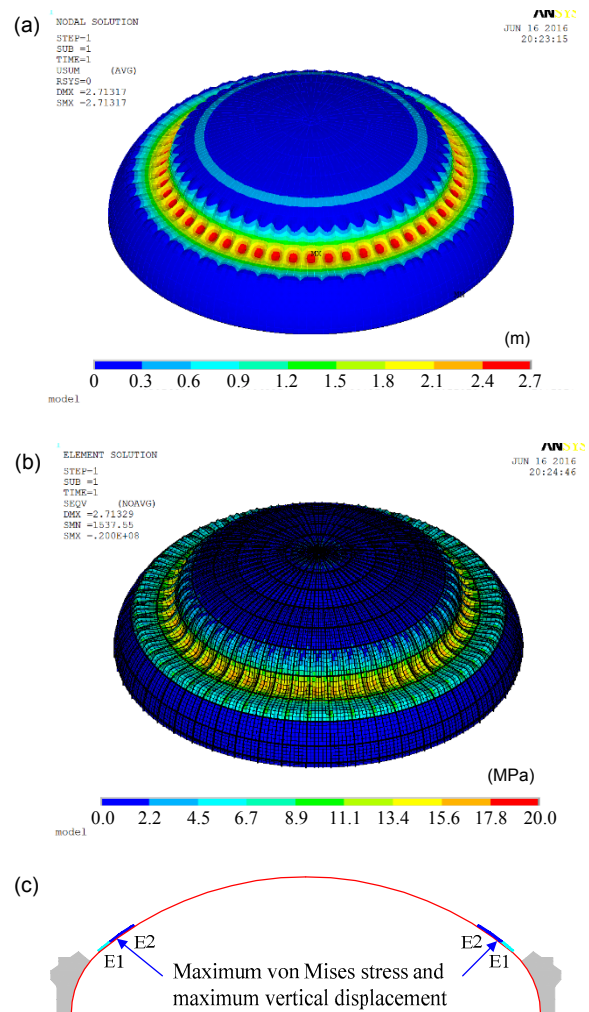
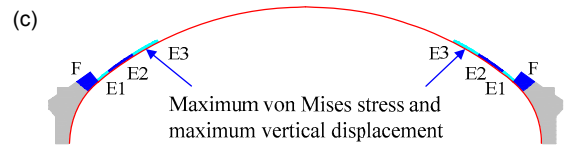
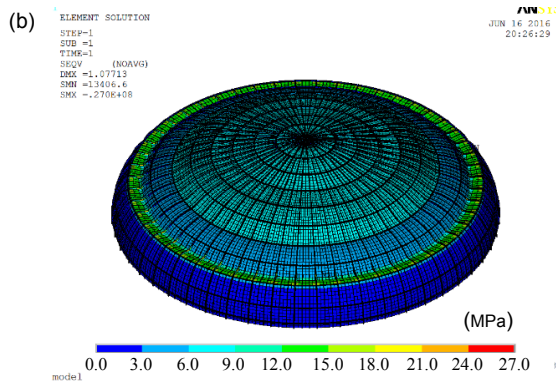
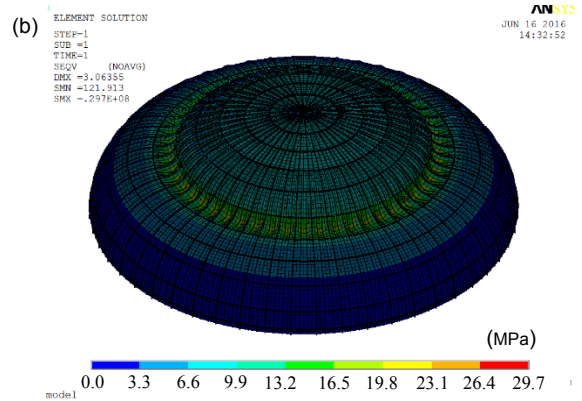
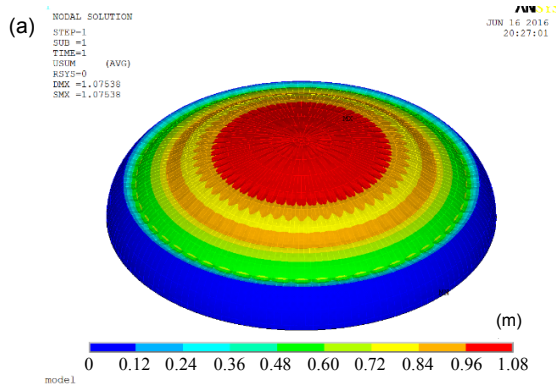


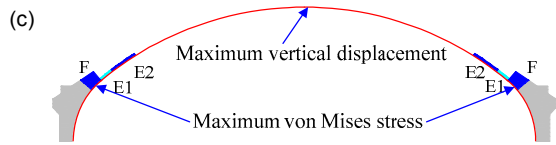
Fig. 13 Position of maximum vertical displacement and von Mises stress of the steel liner at the construction stages E1 and E2

(a) Vertical displacement of the steel liner at the construction stages E1 and E2; (b) von Mises stress of the steel liner at the construction stages E1 and E2; (c) Position of maximum vertical displacement and von Mises stress of the steel liner at the construction stages E1 and E2



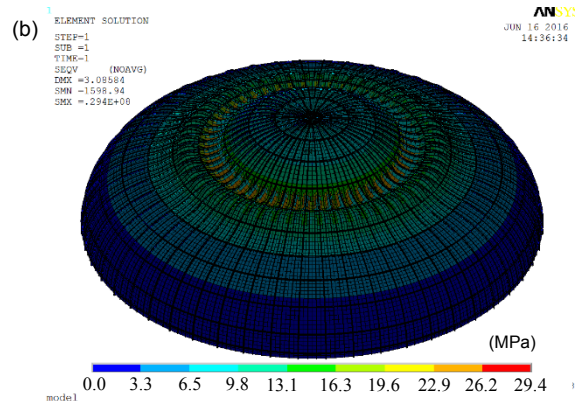
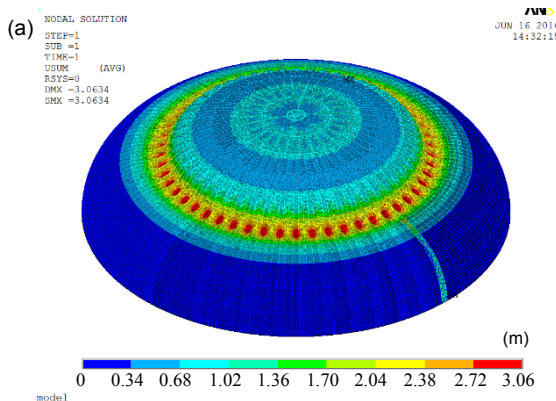
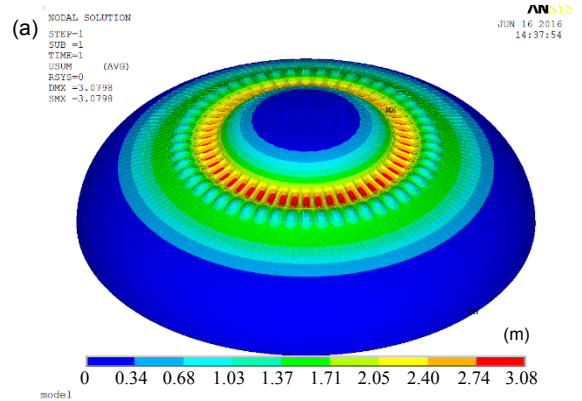
**Fig. 15** Vertical displacement and von Mises stress of the steel liner at the construction stage E3

(a) Vertical displacement of the steel liner at the construction stage E3; (b) von Mises stress of the steel liner at the construction stage E3; (c) Position of maximum vertical displacement and von Mises stress of the steel liner at the construction stage E3



**Fig. 14** Vertical displacement and von Mises stress of the steel liner at the construction stage F

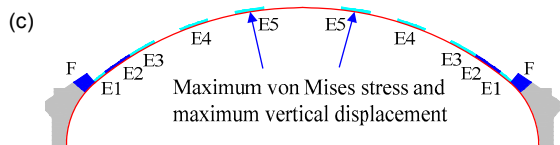
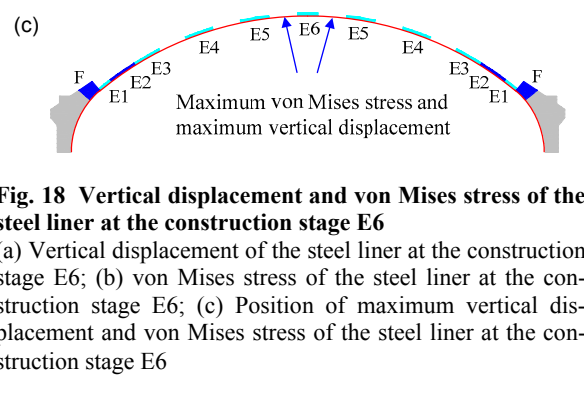
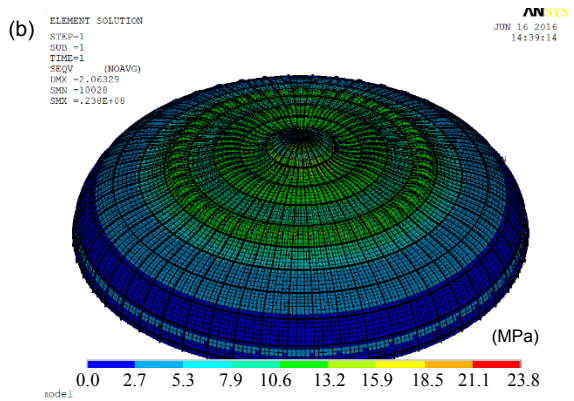
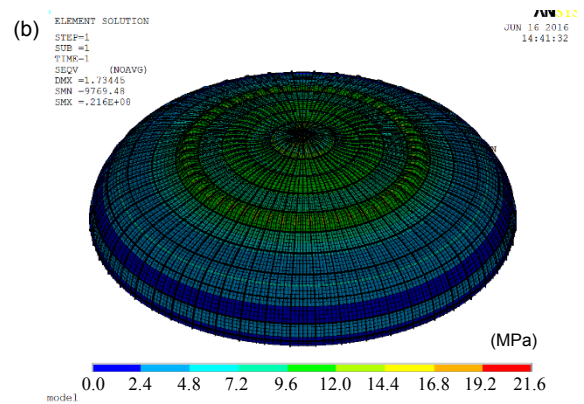
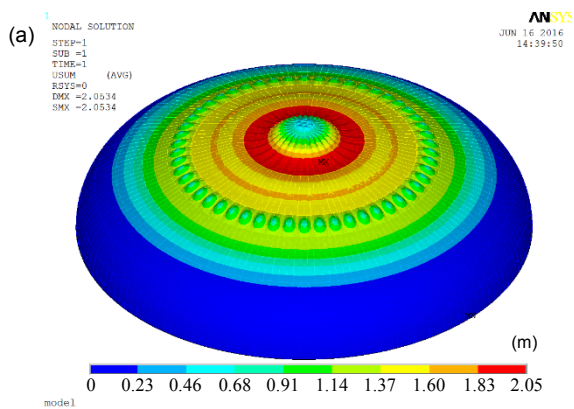
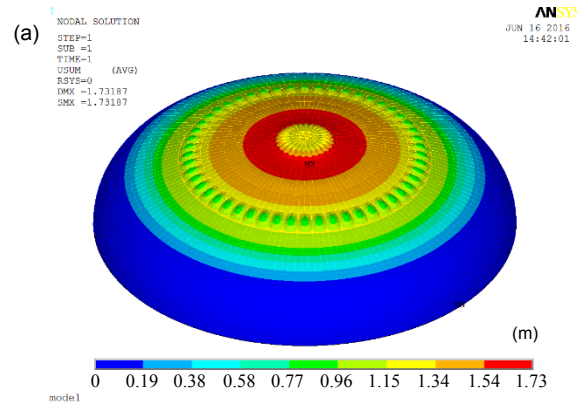
(a) Vertical displacement of the steel liner at the construction stage F; (b) von Mises stress of the steel liner at the construction stage F; (c) Position of maximum vertical displacement and von Mises stress of the steel liner at the construction stage F





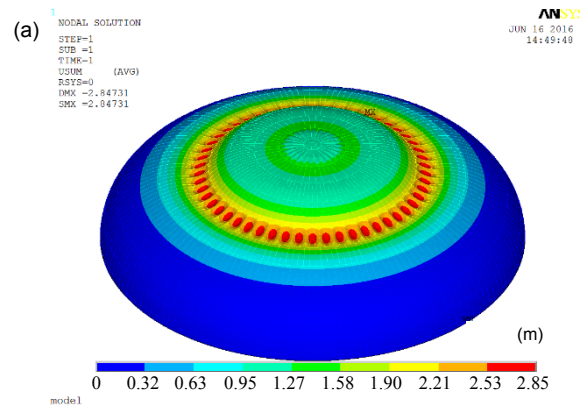
**Fig. 16 Vertical displacement and von Mises stress of the steel liner at the construction stage E4**

(a) Vertical displacement of the steel liner at the construction stage E4; (b) von Mises stress of the steel liner at the construction stage E4; (c) Position of maximum vertical displacement and von Mises stress of the steel liner at the construction stage E4



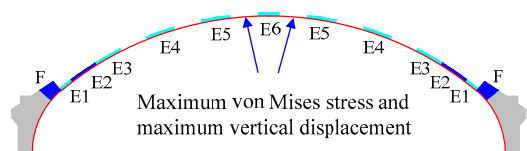
**Fig. 17 Vertical displacement and von Mises stress of the steel liner at the construction stage E5**

(a) Vertical displacement of the steel liner at the construction stage E5; (b) von Mises stress of the steel liner at the construction stage E5; (c) Position of maximum vertical displacement and von Mises stress of the steel liner at the construction stage E5



**Fig. 18 Vertical displacement and von Mises stress of the steel liner at the construction stage E6**

(a) Vertical displacement of the steel liner at the construction stage E6; (b) von Mises stress of the steel liner at the construction stage E6; (c) Position of maximum vertical displacement and von Mises stress of the steel liner at the construction stage E6



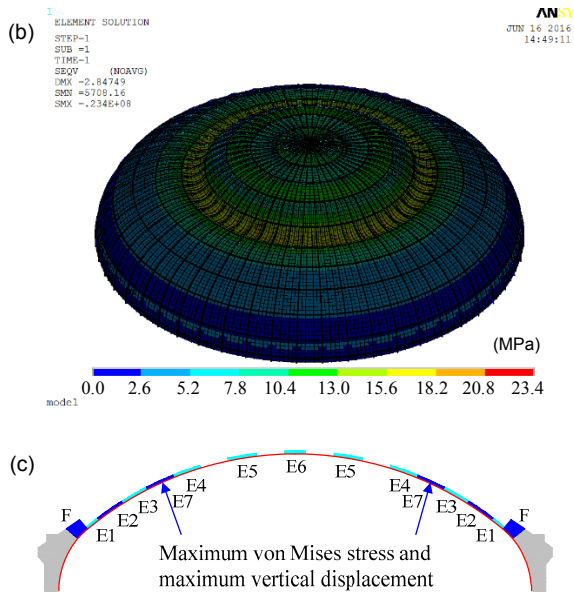


**Fig. 19** Vertical displacement and von Mises stress of the steel liner at the construction stage E7

(a) Vertical displacement of the steel liner at the construction stage E7; (b) von Mises stress of the steel liner at the construction stage E7; (c) Position of maximum vertical displacement and von Mises stress of the steel liner at the construction stage E7

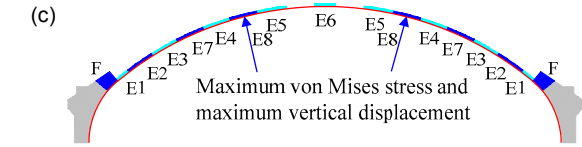
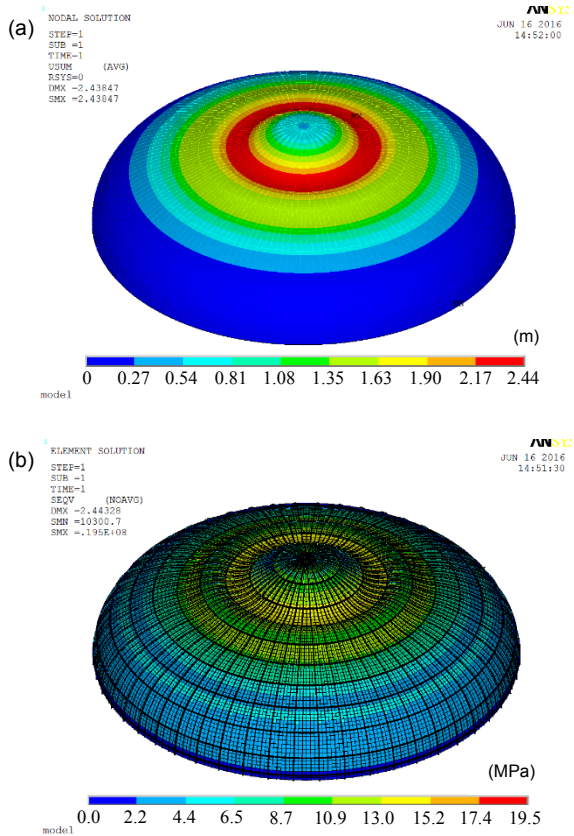


**Fig. 20** Vertical displacement and von Mises stress of the steel liner at the construction stage E8

(a) Vertical displacement of the steel liner at the construction stage E8; (b) von Mises stress of the steel liner at the construction stage E8; (c) Position of maximum vertical displacement and von Mises stress of the steel liner at the construction stage E8

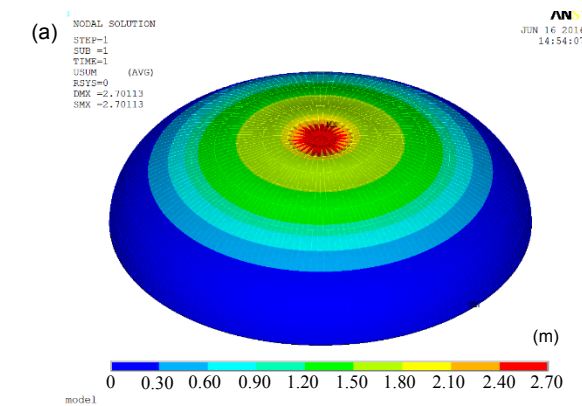


**Fig. 21** Vertical displacement and von Mises stress of the steel liner at the construction stage E9

(a) Vertical displacement of the steel liner at the construction stage E9; (b) von Mises stress of the steel liner at the construction stage E9; (c) Position of maximum vertical displacement and von Mises stress of the steel liner at the construction stage E9

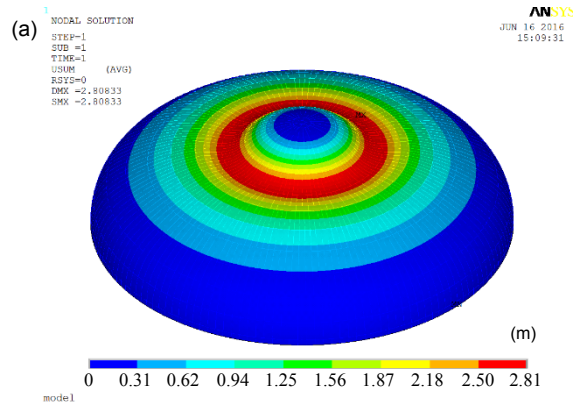
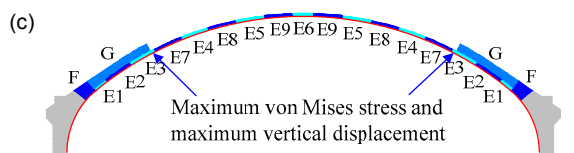
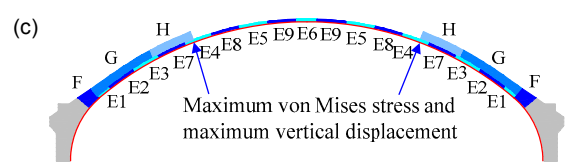
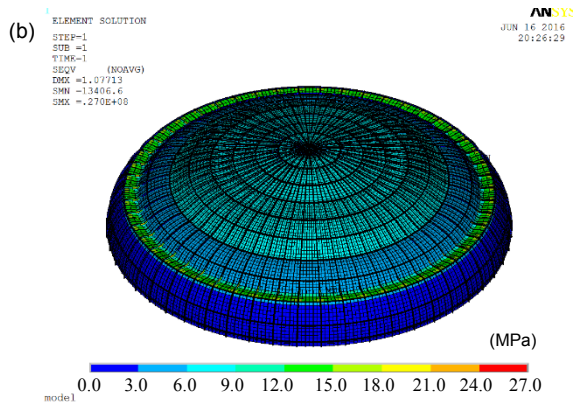
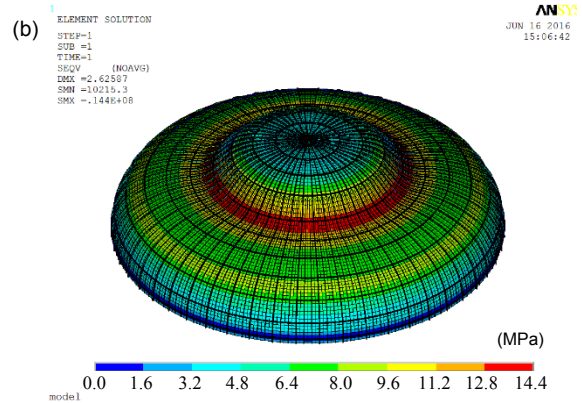
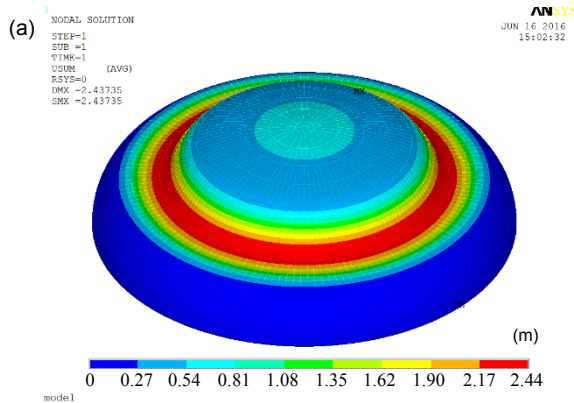


**Fig. 22 Vertical displacement and von Mises stress of the steel liner at the construction stage G**

(a) Vertical displacement of the steel liner at the construction stage G; (b) von Mises stress of the steel liner at the construction stage G; (c) Position of maximum vertical displacement and von Mises stress of the steel liner at the construction stage G

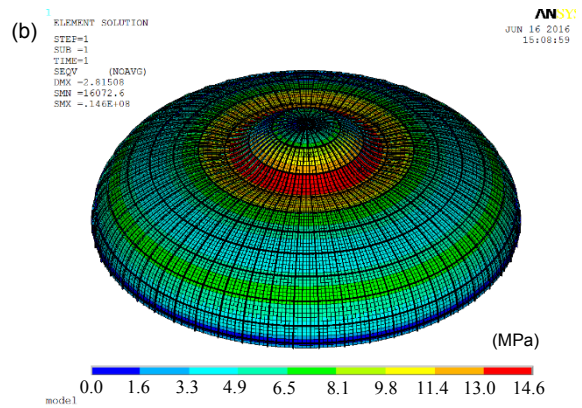
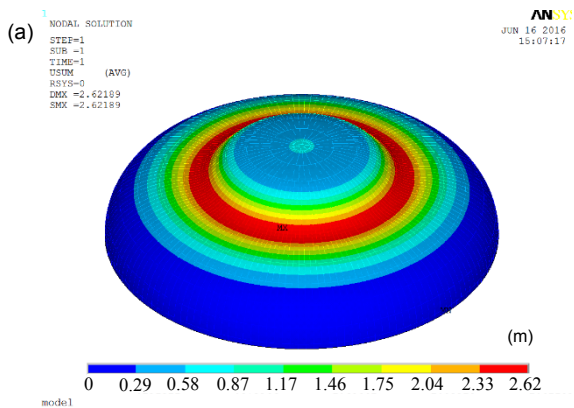


**Fig. 23 Vertical displacement and von Mises stress of the steel liner at the construction stage H**

(a) Vertical displacement of the steel liner at the construction stage H; (b) von Mises stress of the steel liner at the construction stage H; (c) Position of maximum vertical displacement and von Mises stress of the steel liner at the construction stage H

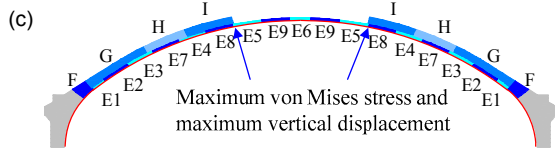


**Fig. 24 Vertical displacement and von Mises stress of the steel liner at the construction stage I**

(a) Vertical displacement of the steel liner at the construction stage I; (b) von Mises stress of the steel liner at the construction stage I; (c) Position of maximum vertical displacement and von Mises stress of the steel liner at the construction stage I

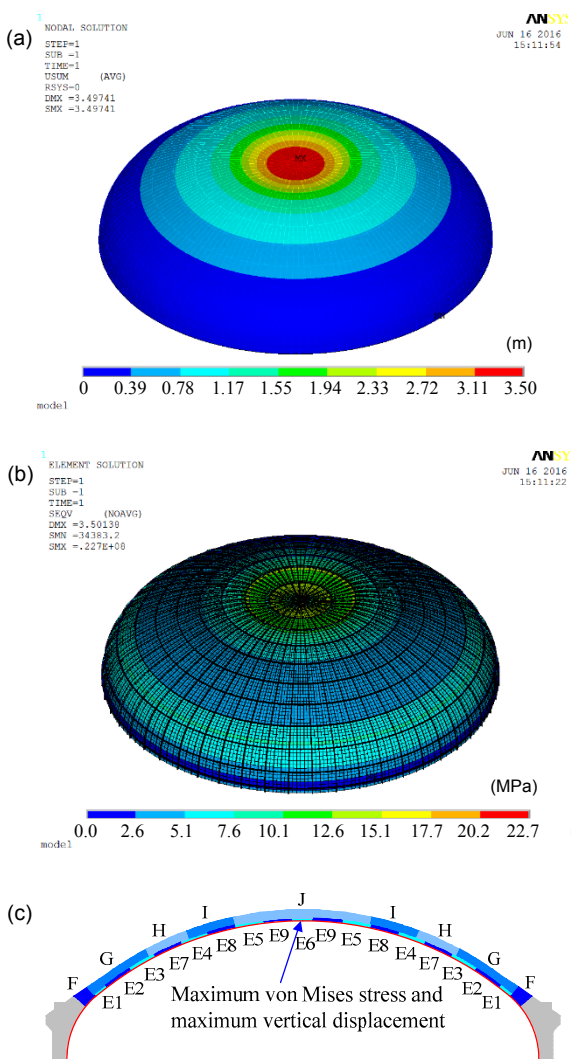


**Fig. 25 Vertical displacement and von Mises stress of the steel liner at the construction stage J**

(a) Vertical displacement of the steel liner at the construction stage J; (b) von Mises stress of the steel liner at the construction stage J; (c) Position of maximum vertical displacement and von Mises stress of the steel liner at the construction stage J

steel liner can be seen to change gradually with the pouring and hardening of each subsequent concrete layer.

The first-order principle tensile stress and first-order principle compressive stress histories of concrete during different construction stages are shown in Fig. 26. According to the simulation for pouring concrete on the dome containment, both the maximum tensile stress and the maximum compressive stress of the concrete are less than 1.0 MPa, which indicates that concrete cracking will not occur.

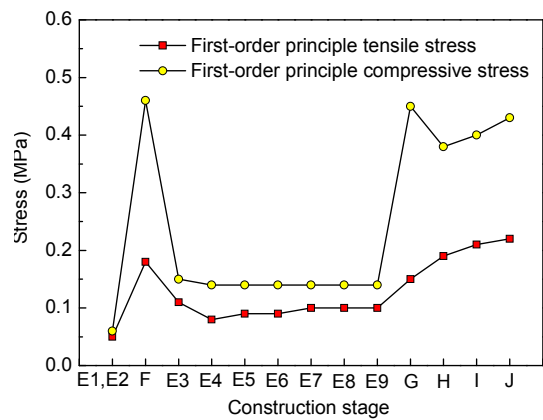


**Fig. 26 First-order principle tensile stress and principle compressive stress of the concrete during different construction stages**

The membrane internal force is the primary internal force on the steel dome liner. The maximum von Mises stresses of the steel plates and the angle steel stiffeners are about 25.7 MPa and 40.4 MPa, respectively (Fig. 27). The maximum vertical displacement of the structure is 3.50 mm, which satisfies the deformation requirement (Fig. 28).

**5.2 Structural stability analysis during construction**

A buckling failure of the structure can occur suddenly, which often leads to catastrophic accidents (Gioncu, 1995). For the inner containment of an EPR nuclear power plant, a buckling failure may occur in the construction phase. During the whole construction process for the concrete pouring on the steel dome liner, a buckling failure may happen in two key phases. The first key phase is the concrete pouring for the 200 mm thick concrete bottom on the steel dome liner, when the gravity of the 200 mm thick concrete bottom is applied on the steel dome liner as the load. For this phase, the steel dome liner

is the concrete formwork. The steel dome liner is the only supporting structure for the concrete pouring, while no vertical support is provided to support the steel dome liner. The second key phase is the concrete pouring of 0.80 m thick concrete from layer G to layer J (Fig. 11), which means the gravity of the 0.80 m thick concrete is applied on the steel-concrete composite dome as the load. The steel-concrete composite dome is composed of the steel dome liner and the 200 mm thick concrete bottom. During this phase, with the hardening of the poured concrete, the steel dome liner structure is converted into the steel-concrete composite dome structure to resist the gravity load of the newly poured concrete. It can be analyzed that, for these two phases, the formwork in construction is different. The concrete formworks for the first and the second phases are the steel dome liner and the steel-concrete composite dome, respectively.

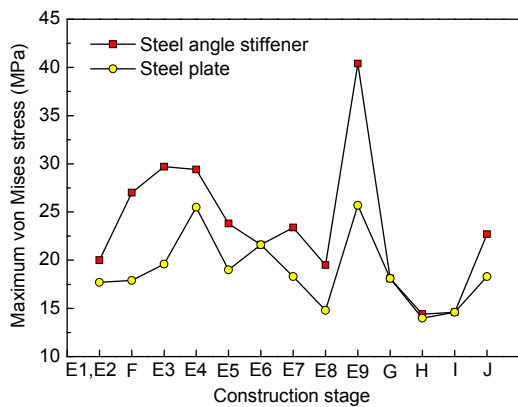


Fig. 27 Maximum von Mises stress of the steel liner during different construction stages

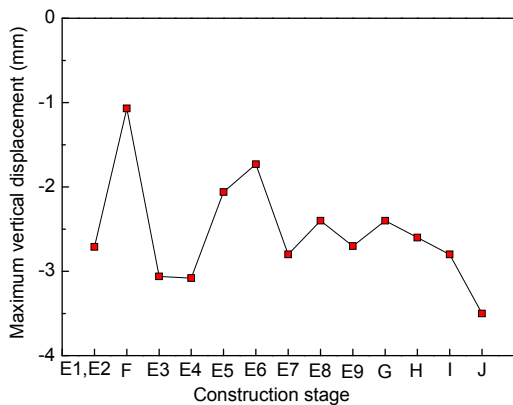


Fig. 28 Maximum vertical displacement of the steel liner during different construction stages

According to the Chinese code “Technical Code for Safety of Forms in Construction” (JGJ162-2008) (MOHURD, 2008), for the stability analysis of the formwork structure, the dead load is the weight of the steel dome liner and the poured concrete, and the live load is the weight of the constructors and equipment. For the inner containment of the Taishan nuclear power project, the live load is taken as 4.0 kN/m<sup>2</sup> along the projected area. That is, along the surface area of the shell, the equivalent uniformly distributed live load is 2.78 kN/m<sup>2</sup>. According to the Chinese code “Technical Specification for Space Frame Structures” (JGJ7-2010) (MOHURD, 2010), the influence of the unsymmetrical distribution of load on the stability of the dome structure is negligible. The stability-bearing capacity of the structure can be measured by the characteristic combination of the dead load and the live load. When the uniformly distributed vertical load is applied along the whole span of the structure, the allowable bearing capacity of the structure equals the stability-bearing capacity divided by the safety factor. When the stability-bearing capacity of the dome is obtained through the geometrically and materially nonlinear analysis of the structure, the safety factor should be more than 2.0.

### 1. Initial geometrical imperfection

The initial geometrical imperfection is inevitable in practice (CEN, 2007). According to the Chinese code “Technical Specification for Space Frame Structures” (JGJ7-2010) (MOHURD, 2010), the lowest-order buckling mode is recommended to simulate the initial geometrical imperfection distribution. Shen and Chen (1999) proposes to conduct the nonlinear whole-course analysis for the ideal structure to obtain the lowest-order buckling mode of the structure, and then introduce the lowest-order buckling mode as the initial geometrical imperfection distribution. The results show that this simulation method is valid to introduce the initial geometrical imperfection of the structure.

### 2. Stability bearing capacity of the structure during construction

Along the surface area of the shell, the dead load of the steel dome liner is about 0.72 kN/m<sup>2</sup>; the dead load of the newly pouring of 0.20 m thick concrete is 4.70 kN/m<sup>2</sup>; the dead load of the newly pouring of 0.80 m thick concrete is 18.80 kN/m<sup>2</sup>; the

standard value of the live load is  $2.78 \text{ kN/m}^2$ . The lowest-order buckling mode of the structure obtained from the nonlinear whole-course analysis for the ideal structure is used as the initial geometrical imperfection distribution, and the maximum value of the initial geometrical imperfection is  $1/300$  of the span of the structure.

(1) For the stability analysis of the structure during the first key phase, when the concrete bottom (0.20 m thick) is poured on the steel dome liner, the stability-bearing capacity of the structure is  $26.9 \text{ kN/m}^2$ , and the safety factor is 3.50.

(2) For the stability analysis of the structure during the second key phase, the concrete bottom (0.20 m thick) hardens and the steel-concrete composite dome is shaped. When 0.80 m thick concrete is poured on the composite dome, the stability-bearing capacity of the structure is  $77.8 \text{ kN/m}^2$ , and the safety factor is 3.60.

During the construction of the inner containment, for the two key phases, the stability behaviors of the different structures are similar. According to the analysis, the structural stability-bearing capacity satisfies the requirements of the Chinese code "Technical Specification for Space Frame Structures" (JGJ7-2010) (MOHURD, 2010), which means that the construction scheme is reasonable.

## 6 Conclusions

In considering the application of modular construction technology for the steel liner of the inner containment structure, three key problems were identified and analyzed in detail.

Compared with the circular space truss with the quadrilateral cross section, new lifting equipment using a circular space truss with the triangular cross section is proposed, which can satisfy stress and deformation requirements and can reduce steel consumption by approximately 20.0%. During the lifting of the dome module, the maximum vertical deformation is only 1.30 mm without the vertical rigid body displacement. In addition, the maximum von Mises stress of the lifting lug is 115 MPa. During the lifting of the dome module, the working wind speed should be controlled to within 6.17 m/s.

The relationship between the steel cylinder liner modular height and the maximum height of each concrete pouring was determined. The result shows that the height of the steel cylinder liner module can be increased if the capacity of the crane is sufficient.

The "overlapping element and birth-death element" technique was adopted to simulate the construction process for concrete pouring, while the calculation for a load step was based on the calculation for the previous step. The mechanical properties of the steel dome liner after the concrete pouring were obtained. Two key phases were defined for the stability analysis of the steel dome liner during the whole construction process encompassing the concrete pouring on the steel dome liner, and the corresponding stability analyses were carried out. The results show that the construction scheme is reasonable.

Based on the finite element method, a practical method of modeling and nonlinear analysis is proposed, which provides guidance on the design and analysis for the construction of the containment structure.

## References

- ABAQUS Inc., 2012. Abaqus Theory Manual, Release 6.12. ABAQUS Inc.
- Anderson, P., 2005. Thirty years of measured prestress at Swedish nuclear reactor containments. *Nuclear Engineering and Design*, **235**(21):2323-2336.
- ANSYS Inc., 2012. Ansys Theory Manual, Release 14.5. ANSYS Inc.
- ASME (American Society of Mechanical Engineers), 2015. BPVC Section III-Rules for Construction of Nuclear Facility Components-Division 2-Code for Concrete Containments, BPVC-III-2. ASME.
- ASN (French Nuclear Safety Authority), 2015. EPR Information Letter No. 17: ASN Monitoring of the Flamanville EPR Reactor Construction Site: Notable Points. ASN.  
<http://www.french-nuclear-safety.fr/Inspections/Supervision-of-the-epr-reactor/ASN-s-supervision-of-the-Flamanville-3-reactor-construction-EPR-News/EPR-Information-Letter-No.17#bottom>
- Basha, S.M., Singh, R.K., Patnaik, R., et al., 2003. Predictions of ultimate load capacity for pre-stressed concrete containment vessel model with BARC finite element code ULCA. *Annals of Nuclear Energy*, **30**(4):437-471.  
[http://dx.doi.org/10.1016/S0306-4549\(02\)00075-0](http://dx.doi.org/10.1016/S0306-4549(02)00075-0)
- Becue, P., Barre, F., Arbez, P., 2005. Design of the EPR

- containment. *International Association for Bridge and Structural Engineering*, **90**(9):85-92.
- CEN (European Committee for Standardization), 2003. Flat Products Made of Steels for Pressure Purposes. Part 2: Non-alloy and Alloy Steels with Specified Elevated Temperature Properties, BS EN 10028-2:2003. CEN.
- CEN (European Committee for Standardization), 2004. European Standard. 2: Design of Concrete Structures. Part 1-1: General Rules and Rules for Buildings, BS EN 1992-1-1:2004. CEN.
- CEN (European Committee for Standardization), 2005. European Standard. 3: Design of Steel Structures. Part 1-1: General Rules and Rules for Buildings, BS EN 1993-1-1:2005. CEN.
- CEN (European Committee for Standardization), 2007. European Standard. 3: Design of Steel Structures. Part 1-6: Strength and Stability of Shell Structures, BS EN 1993-1-6:2007. CEN.
- de Clercq, G., 2014. EDF Hopes French EPR will Launch before Chinese Reactors. Reuters.  
<http://af.reuters.com/article/commoditiesNews/idAFL6N0Q665C20140731?sp=true>
- Enformable Nuclear News, 2011. Photos of the China's Lifting of Dome at Taishan Nuclear Power Plant. Enformable Nuclear News.  
<http://enformable.com/2011/10/photos-of-the-chinas-lifting-of-dome-at-taishan-nuclear-power-plant/>
- Fib Task Group on Containment Structures, 2001. Nuclear Containments. International Federation for Structural Concrete.
- Gioncu, V., 1995. Buckling of reticulated shells state-of-the-art. *International Journal of Space Structures*, **10**(1):1-46.
- Hessheimer, M.F., Klammer, E.W., Lambert, L.D., et al., 2003. Overpressurization Test of a 1:4-scale Pre-stressed Concrete Containment Vessel Model. Technical Report No. NU-REG/CR-6810, SAND2003-0840P, Nuclear Regulatory Commission, Washington DC, USA; Sandia National Laboratories, Albuquerque, USA; Nuclear Power Engineering Corporation, Japan.
- Horschel, D.S., 1988. Design, Construction, and Instrumentation of a 1:6 Scale Reinforced Concrete Containment Building. Technical Report No. NUREG/CR-5083, SAND88-0030, Nuclear Regulatory Commission, Washington DC, USA; Sandia National Laboratories, Albuquerque, USA.
- Horschel, D.S., 1992. Experimental Results from Pressure Testing of a 1:6 Scale Nuclear Power Plant Containment. Technical Report No. NU-REG/CR-5121, SAND88-0906, Nuclear Regulatory Commission, Washington DC, USA; Sandia National Laboratories, Albuquerque, USA.
- Hu, H.T., Lin, J.X., 2016. Ultimate analysis of PWR prestressed concrete containment under long-term prestressing loss. *Annals of Nuclear Energy*, **87**:500-510.
- IAEA (International Atomic Energy Agency), 2012a. Nuclear Power Reactor Details: Taishan-1. Power Reactor Information System.  
<https://www.iaea.org/PRIS/CountryStatistics/ReactorDetails.aspx?current=918>
- IAEA (International Atomic Energy Agency), 2012b. Nuclear Power Reactor Details: Taishan-2. Power Reactor Information System.  
<https://www.iaea.org/PRIS/CountryStatistics/ReactorDetails.aspx?current=919>
- Kim, S.H., Choi, M.S., Jung, J.Y., et al., 2013. Long-term reliability evaluation of nuclear containments with tendon force degradation. *Nuclear Engineering and Design*, **265**:582-590.  
<http://dx.doi.org/10.1016/j.nucengdes.2013.06.025>
- Kwak, H.G., Kwon, Y., 2016. Nonlinear analysis of containment structure based on modified tendon model. *Annals of Nuclear Energy*, **92**:113-126.  
<http://dx.doi.org/10.1016/j.anucene.2016.01.040>
- Lapp, C.W., Golay, M.W., 1997. Modular design and construction techniques for nuclear power plants. *Nuclear Engineering and Design*, **172**(3):327-349.  
[http://dx.doi.org/10.1016/S0029-5493\(97\)00031-9](http://dx.doi.org/10.1016/S0029-5493(97)00031-9)
- Lee, H.P., Choun, Y.S., Seo, J.M., 2004. Nonlinear finite element analysis of containment vessel by considering the tension stiffening effect. *Journal of the Korean Nuclear Society*, **36**(6):512-527.
- Lundqvist, P., Nilsson, L.O., 2011. Evaluation of prestress losses in nuclear reactor containments. *Nuclear Engineering and Design*, **241**(1):168-176.  
<http://dx.doi.org/10.1016/j.nucengdes.2010.11.007>
- Marques, J.G., 2010. Evolution of nuclear fission reactors: third generation and beyond. *Energy Conversion and Management*, **51**(9):1774-1780.  
<http://dx.doi.org/10.1016/j.enconman.2009.12.043>
- MOHURD (Ministry of Housing and Urban-Rural Development), 2003. Code for Design of Steel Structures, GB50017-2003. National Standards of People's Republic of China (in Chinese).
- MOHURD (Ministry of Housing and Urban-Rural Development), 2008. Technical Code for Safety of Forms in Construction, JGJ 162-2008. Construction Industry Standards of People's Republic of China (in Chinese).
- MOHURD (Ministry of Housing and Urban-Rural Development), 2009. Code for Construction of Mass Concrete, GB50496-2009. National Standards of People's Republic of China (in Chinese).
- MOHURD (Ministry of Housing and Urban-Rural Development), 2010. Technical Specification for Space Frame Structures, JGJ 7-2010. Construction Industry Standards of People's Republic of China (in Chinese).
- MOHURD (Ministry of Housing and Urban-Rural Development), 2012a. Load Code for the Design of Building Structures, GB 50009-2012. National Standards of People's Republic of China (in Chinese).
- MOHURD (Ministry of Housing and Urban-Rural Development), 2012b. Specification for Design of Reinforced Concrete Shell Structures, JGJ 22-2012. Construction

- Industry Standards of People's Republic of China (in Chinese).
- Nuclear Engineering International, 2009. Olkiluoto 3 Reactor Building Gets Roof. Global Trade Media, Progressive Media Group Limited.
- Parmar, R.M., Singh, T., Thangamani, I., et al., 2014. Overpressure test on barcom pre-stressed concrete containment. *Nuclear Engineering and Design*, **269**:177-183. <http://dx.doi.org/10.1016/j.nucengdes.2013.08.027>
- People's Daily, 2009. Taishan Nuclear Power Plant to Be One of World's Largest. People's Daily Online. <http://en.people.cn/90001/90776/90883/6849430.html>
- Rizkalla, S.H., Macgregor, J.G., Simmonds, S.H., 1984. Prestressed concrete containment model. *Journal of Structural Engineering*, **110**(4):730-743. [http://dx.doi.org/10.1061/\(asce\)0733-9445\(1984\)110:4\(730\)](http://dx.doi.org/10.1061/(asce)0733-9445(1984)110:4(730))
- Shen, S.Z., Chen, X., 1999. Stability of Reticulated Shells. Science Press, Beijing, China (in Chinese).
- Shokoohfar, A., Rahai, A., 2016. Nonlinear analysis of pre-stressed concrete containment vessel (PCCV) using the damage plasticity model. *Nuclear Engineering and Design*, **298**:41-50. <http://dx.doi.org/10.1016/j.nucengdes.2015.12.019>
- Timoshenko, S., Woinowsky-Krieger, S., 1959. Theory of Plates and Shells. McGraw-Hill Book Company, USA.
- Twidale, D., Crowder, R., 1991. Sizewell 'B'-A one tenth scale containment model test for the UK PWR programme. *Nuclear Engineering and Design*, **125**(1): 85-93. [http://dx.doi.org/10.1016/0029-5493\(91\)90008-6](http://dx.doi.org/10.1016/0029-5493(91)90008-6)
- von Riesenmann, W.A., Parks, M.B., 1995. Current state of knowledge on the behavior of steel liners in concrete containments subjected to overpressurization loads. *Nuclear Engineering and Design*, **157**(3):481-487. [http://dx.doi.org/10.1016/0029-5493\(95\)01003-Z](http://dx.doi.org/10.1016/0029-5493(95)01003-Z)
- Wang, G.Y., 2000. On mechanics of time-varying structures. *China Civil Engineering Journal*, **33**(6):105-108 (in Chinese).
- WNA (World Nuclear Association), 2010. Nuclear Power in China. WNA.
- WNN (World Nuclear News), 2013a. Symbolic Milestone for Finnish EPR. WNN. [http://www.world-nuclear-news.org/NN-Symbolic\\_milestone\\_for\\_Finnish\\_EPR-2410134.html](http://www.world-nuclear-news.org/NN-Symbolic_milestone_for_Finnish_EPR-2410134.html)
- WNN (World Nuclear News), 2013b. Taishan Generator Stator Lift. WNN. [http://www.world-nuclear-news.org/NN-Taishan\\_generator\\_lift\\_1110131.html](http://www.world-nuclear-news.org/NN-Taishan_generator_lift_1110131.html)
- Yonezawa, K., Imoto, K., Watanabe, Y., et al., 2002. Ultimate capacity analysis of 1/4 PCCV model subjected to internal pressure. *Nuclear Engineering and Design*, **212**(1-3):357-379. [http://dx.doi.org/10.1016/S0029-5493\(01\)00498-8](http://dx.doi.org/10.1016/S0029-5493(01)00498-8)
- Zhang, X., 2009. 900 MW PWR containment mechanical behavior characteristics during containment test. *Nuclear Engineering and Design*, **239**(9):1647-1652. <http://dx.doi.org/10.1016/j.nucengdes.2009.04.003>

## 中文概要

**题目:** 欧洲压水堆核电站安全壳钢衬里模块化施工力学研究

**目的:** 以广东台山欧洲压水堆(EPR)核电站安全壳钢衬里结构为研究背景,提炼钢衬里结构模块化施工全过程中的关键力学问题,对钢衬里结构模块化施工技术从力学角度给出建议,对确定结构施工方案和保证结构施工安全具有实用参考价值。

**创新点:** 1. 提炼出 EPR 核电站安全壳钢衬里结构模块化施工全过程中的关键力学问题; 2. 采用“重叠单元和生死单元”技术模拟大型复杂结构混凝土浇筑成型全过程。

**方法:** 1. 通过精细化有限元分析,开展吊装工装结构优化分析、吊耳节点多尺度有限元分析和工作风速分析; 2. 建立安全壳结构复杂实体有限元模型,分析模块之间对接拼装初内力、新浇筑混凝土侧压力、不均匀温度作用及风荷载等施工因素对筒体钢衬里的影响; 3. 采用“重叠单元和生死单元”技术,分析大跨度穹顶钢衬里结构在混凝土浇筑成型全过程中的结构变形和应力; 4. 考虑结构初始几何缺陷和材料弹塑性的影响,对混凝土浇筑成型过程中穹顶钢衬里结构进行稳定性分析。

**结论:** 1. 采用三角形环形桁架吊装工装,能够满足吊装过程的应力和变形要求,并减少吊装工装用钢量; 2. 获得了筒体钢衬里模块高度和混凝土一次浇筑最大高度的相关曲线; 3. 得到了混凝土浇筑成型全过程中穹顶钢衬里结构的力学性能; 4. 定义并验算了混凝土浇筑成型过程中穹顶钢衬里结构两个关键阶段的稳定性,为此类结构施工提供了理论参考。

**关键词:** 安全壳; 施工力学; 钢衬里; 重叠单元; 生死单元